Nonlinear Dyn (2023) 111:5709–5720
https://doi.org/10.1007/s11071-022-08134-7

ORIGINAL PAPER

Localized wave solutions to a variable-coefficient coupled Hirota equation in inhomogeneous optical fiber

N. Song · H. J. Shang · Y. F. Zhang · W. X. Ma

Received: 7 October 2022 / Accepted: 24 November 2022 / Published online: 7 December 2022

Abstract The first- and second-order localized waves for a variable-coefficient coupled Hirota equation describe the vector optical pulses in inhomogeneous optical fiber and are investigated via generalized Darboux transformation in this work. Based on the equation's Lax pair and seed solutions, the localized wave solutions are calculated, and the dynamics of the obtained localized waves are shown and analyzed through numerical simulation. A series of novel dynamical evolution plots illustrating the interaction between the rogue waves and dark-bright solitons or breathers are provided. It is found that functions have an influence on the propagation of shape, period, and velocity of the localized waves. The presented results contribute to enriching the dynamics of localized waves in inhomogeneous optical fiber.

Keywords Variable-coefficient coupled Hirota equation · Generalized Darboux transformation · Soliton · Breather

N. Song (✉) · H. J. Shang · Y. F. Zhang
School of Mathematics, North University of China, Taiyuan 030051, Shanxi, China
e-mail: songni@nuc.edu.cn

W. X. Ma
Department of Mathematics, Zhejiang Normal University, Jinhua 321004, Zhejiang, China

W. X. Ma
Department of Mathematics, King Abdulaziz University, Jeddah 21589, Saudi Arabia

W. X. Ma
Department of Mathematics and Statistics, University of South Florida, Tampa, FL 33620-5700, USA

W. X. Ma (✉)
School of Mathematical and Statistical Sciences, North-West University, Mafikeng Campus, Private Bag X2046, Mmabatho 2735, South Africa
e-mail: mawx@cas.usf.edu

1 Introduction

As the primary tool for transmitting various types of information, optical fiber communication has a wide range of applications and is developing rapidly [1–5]. In recent years, an increasing number of researchers have devoted themselves to studying the dynamics of nonlinear evolution equations in the field of optics, including the nonlinear Schrödinger equation [6–8], the Kundu-Eckhaus equation [9,10], the Radhakrishnan-Kundu-Lakshmanan equation [11], the complex cubic quintic Ginzburg-Landau equation [12], and the Gerdjikov-Ivanov equation [13]. Scholars have switched their attention from constant-coefficient equations [14,15] to variable-coefficient equations [16–18], which more effectively account for the inhomogeneity of the medium and its nonuniform boundaries. The variable-coefficient equations were then applied to describe localized waves, which consist of solitons [19,20], breathers [21], and rogue waves [22,23]. Several methods are used to investigate localized waves, including Darboux transformation (DT) [24–26], Bäcklund transformation [27], bilinear methods [28,29], and the unified method [30]. The study of localized waves in nonlinear optical fiber using variable-coefficient equations have provided the theoretical basis for modern communication [31,32].

Motivated by the above considerations, a variable-coefficient coupled Hirota equation is studied in this work [33]:

$$
\begin{aligned}
& i q_{1t}+\alpha(t) q_{1xx}+2\beta(t)(|q_1|^2+|q_2|^2) q_1 \\
& +i\delta(t)\left[\frac{\beta(t)}{\alpha(t)}(6|q_1|^2+3|q_2|^2) q_{1x}\right. \\
& \left.+3\frac{\beta(t)}{\alpha(t)} q_1 q_2^* q_{2x}+q_{1xxx}\right] \\
& +\frac{1}{2} i\left\{\frac{[\beta(t)]_t}{\beta(t)}-\frac{[\alpha(t)]_t}{\alpha(t)}\right\} q_1=0,
\end{aligned} \tag{1a}
$$

$$
\begin{aligned}
& i q_{2t}+\alpha(t) q_{2xx}+2\beta(t)(|q_1|^2+|q_2|^2) q_2 \\
& +i\delta(t)\left[\frac{\beta(t)}{\alpha(t)}(6|q_2|^2+3|q_1|^2) q_{2x}\right. \\
& \left.+3\frac{\beta(t)}{\alpha(t)} q_2 q_1^* q_{1x}+q_{2xxx}\right] \\
& +\frac{1}{2} i\left\{\frac{[\beta(t)]_t}{\beta(t)}-\frac{[\alpha(t)]_t}{\alpha(t)}\right\} q_2=0,
\end{aligned} \tag{1b}
$$

where q_j $(j=1,2)$ is the complex envelope in the electric field, x is the evolution time, t is the propagation distance, and $*$ denotes a complex conjugate. Additionally, $\alpha(t)$, $\beta(t)$, $\delta(t)$, $\frac{\beta(t)}{\alpha(t)}$, and $\frac{1}{2}\left\{\frac{[\beta(t)]_t}{\beta(t)}-\frac{[\alpha(t)]_t}{\alpha(t)}\right\}$ are the coefficients of group velocity dispersion (GVD), the nonlinear terms referring to self-phase modulation (SPM) and cross-phase modulation (XPM), the third-order dispersion (TOD), nonlinear terms related to self-steepening and delayed nonlinear response, and the gain or absorption modulus, respectively.

Previous research on Eq. (1) has been carried out, in which two types of Nth-order rogue wave solutions with different dynamic structures were considered [34]. Optical vector breather solutions were obtained via DT as a symbolic iteration technique [35]. Shi et al. obtained the polynomial wave solutions and the rational wave solutions via a unified method [36]. Yang et al. derived one- and two-fold soliton solutions and one- and two-fold breather solutions [37]. Further, Yang et al. presented one- and two-fold breather-to-soliton conversion conditions [38].

Studies demonstrate that multi-wave interaction enriches the research results of nonlinear evolution equations and produces complementary effects in some coupled or vector systems [39–41]. Thus, unlike the above existing research results on Eq. (1), the dynamical characteristics of first- and second-order localized waves will be investigated in this paper. In the present work, the generalized DT is derived, and the dynamics of first- and second-order localized wave solutions are discussed by combining the classical DT and limit methods.

The remainder of this paper is organized as follows. In Sect. 2, the generalized DT is derived, and the higher-order localized wave solutions are obtained. Based on numerical simulation, the evolution plots of the first- and second-order localized waves are given in Sect. 3, and their dynamical characteristics are discussed. Finally, Sect. 4 provides several conclusions.

2 Generalized Darboux transformation

The generalized DT is an effective method for solving nonlinear evolution equations. In this section, the generalized DT is derived, and the iterative formula of the Nth-order solutions is obtained for Eq. (1).

The following Lax pair of Eq. (1) is considered [38]:

$$\Phi_x = U\Phi, \tag{2a}$$

$$\Phi_t = V\Phi, \tag{2b}$$

where

$$U=\lambda\sigma+U_1,\ V=\lambda^3V_1+\lambda^2V_2+\lambda V_3+V_4,$$
$$\sigma=\begin{pmatrix}-2i&0&0\\0&i&0\\0&0&i\end{pmatrix},\ U_1=i\sqrt{\frac{\beta(t)}{\alpha(t)}}\begin{pmatrix}0&q_1&q_2\\q_1^*&0&0\\q_2^*&0&0\end{pmatrix},$$
$$V_1=9\delta(t)\sigma,\ V_2=3\alpha(t)\sigma+9\delta(t)U_1,$$
$$V_3=3i\begin{pmatrix}\frac{\beta(t)\delta(t)}{\alpha(t)}(|q_1|^2+|q_2|^2) & \sqrt{\frac{\beta(t)}{\alpha(t)}}\left[q_1\alpha(t)+i\delta(t)q_{1x}\right] & \sqrt{\frac{\beta(t)}{\alpha(t)}}\left[q_2\alpha(t)+i\delta(t)q_{2x}\right]\\ \sqrt{\frac{\beta(t)}{\alpha(t)}}\left[q_1^*\alpha(t)-i\delta(t)q_{1x}^*\right] & -\frac{\beta(t)\delta(t)}{\alpha(t)}|q_1|^2 & -\frac{\beta(t)\delta(t)}{\alpha(t)}q_1^*q_2\\ \sqrt{\frac{\beta(t)}{\alpha(t)}}\left[q_2^*\alpha(t)-i\delta(t)q_{2x}^*\right] & -\frac{\beta(t)\delta(t)}{\alpha(t)}q_2^*q_1 & -\frac{\beta(t)\delta(t)}{\alpha(t)}|q_2|^2\end{pmatrix},$$
$$V_4=\frac{1}{\alpha(t)}\begin{pmatrix}\beta(t)\left[d_5-\delta(t)(d_{31}+d_{32})\right] & i\sqrt{\frac{\beta(t)}{\alpha(t)}}\left[d_{11}-\alpha(t)d_{21}\right] & i\sqrt{\frac{\beta(t)}{\alpha(t)}}\left[d_{12}-\alpha(t)d_{22}\right]\\ i\sqrt{\frac{\beta(t)}{\alpha(t)}}\left[d_{11}^*-\alpha(t)d_{21}^*\right] & \beta(t)\left[\delta(t)d_{31}-i\alpha(t)|q_1|^2\right] & \beta(t)\left[\delta(t)d_{41}-i\alpha(t)q_1^*q_2\right]\\ i\sqrt{\frac{\beta(t)}{\alpha(t)}}\left[d_{12}^*-\alpha(t)d_{22}^*\right] & \beta(t)\left[\delta(t)d_{42}-i\alpha(t)q_2^*q_1\right] & \beta(t)\left[\delta(t)d_{32}-i\alpha(t)|q_2|^2\right]\end{pmatrix},$$
$$d_{11}=-2\delta(t)\beta(t)q_1\left(|q_1|^2+|q_2|^2\right),$$
$$d_{21}=-i\alpha(t)q_{1x}+\delta(t)q_{1xx},\ d_{31}=q_1^*q_{1x}-q_1q_{1x}^*,$$
$$d_{12}=-2\delta(t)\beta(t)q_2\left(|q_1|^2+|q_2|^2\right),$$
$$d_{22}=-i\alpha(t)q_{2x}+\delta(t)q_{2xx},\ d_{32}=q_2^*q_{2x}-q_2q_{2x}^*,$$
$$d_{41}=q_1^*q_{2x}-q_2q_{1x}^*,\ d_{42}=q_2^*q_{1x}-q_1q_{2x}^*,$$
$$d_5=i\alpha(t)\left(|q_1|^2+|q_2|^2\right),$$

where λ is the spectral parameter, $\Phi=(\varphi,\chi,\phi)^T$ is the vector solution of Eq. (2), and T denotes the transpose for a vector. It is easy to verify that U and V satisfy the compatibility condition $U_t-V_x+[U,V]=0$.

The Darboux matrix T is constructed as follows [42]:

$$T=\lambda I-H\Lambda H^{-1}, \tag{3}$$

where

$$H=\begin{pmatrix}\varphi_1&\chi_1^*&\phi_1^*\\\chi_1&-\varphi_1^*&0\\\phi_1&0&-\varphi_1^*\end{pmatrix},\ \Lambda=\begin{pmatrix}\lambda_1&0&0\\0&\lambda_1^*&0\\0&0&\lambda_1^*\end{pmatrix},$$

in which Φ=$(\varphi_1,\chi_1,\phi_1)^T$ is the eigenfunction of Eq. (2) corresponding to the spectral parameter λ=λ_1, the seed solutions $q_1=q_1[0]$ and $q_2=q_2[0]$, and I is the identity matrix. Thus, the classical DT is defined as:

$$\lambda=\lambda_k,\ \Phi_k=(\varphi_k,\chi_k,\phi_k)^T,\ (k=1,2,\cdots,N), \tag{4}$$
$$\Phi_N[N-1]=T[N-1]T[N-2]\cdots T[1]\Phi_N, \tag{5}$$

$$q_1[N]=q_1[0]-3\sqrt{\frac{\alpha(t)}{\beta(t)}}\sum_{k=1}^{N}(\lambda_1-\lambda_1^*)\times\frac{\varphi_k[k-1]\chi_k^*[k-1]}{|\varphi_k[k-1]|^2+|\chi_k[k-1]|^2+|\phi_k[k-1]|^2}, \tag{6a}$$

$$q_2[N]=q_2[0]-3\sqrt{\frac{\alpha(t)}{\beta(t)}}\sum_{k=1}^{N}(\lambda_1-\lambda_1^*)\times\frac{\varphi_k[k-1]\phi_k^*[k-1]}{|\varphi_k[k-1]|^2+|\chi_k[k-1]|^2+|\phi_k[k-1]|^2}, \tag{6b}$$

where

$$T[k]=\lambda_{k+1}I-H[k-1]\Lambda[k]H[k-1]^{-1},$$
$$\Phi_k[k-1]=(T[k-1]T[k-2]\cdots T[1])\big|_{\lambda=\lambda_k}\Phi_k,$$
$$H[k-1]=\begin{pmatrix}\varphi_k[k-1]&\chi_k^*[k-1]&\phi_k^*[k-1]\\\chi_k[k-1]&-\varphi_k^*[k-1]&0\\\phi_k[k-1]&0&-\varphi_k^*[k-1]\end{pmatrix},$$

$$\Lambda[k]=\begin{pmatrix}\lambda_k & 0 & 0\\ 0 & \lambda_k^* & 0\\ 0 & 0 & \lambda_k^*\end{pmatrix}.$$

The generalized DT of Eq. (1) is constructed based on the above classical DT. Assuming $\Phi_1=\Phi_1(\lambda_1,\eta)$ is a solution of Eq. (2) and η is a small parameter, the following Taylor expansion of η=0 is obtained:

$$\Phi_1=\Phi_1^{[0]}+\Phi_1^{[1]}\eta+\Phi_1^{[2]}\eta^2+\cdots+\Phi_1^{[N]}\eta^N+o\left(\eta^N\right), \tag{7}$$

where

$$\Phi_1^{[k]}=\frac{1}{k!}\frac{\partial^k}{\partial\lambda^k}\Phi_1(\lambda)\,|_{\lambda=\lambda_1}=\left(\varphi_1^{[k]},\chi_1^{[k]},\phi_1^{[k]}\right)^T,\quad (k=0,1,2,\cdots,N).$$

It can be easily confirmed that $\Phi_1^{[0]}=\Phi_1[0]$ is a special solution with λ=λ_1, $q_1=q_1[0]$, and $q_2=q_2[0]$ of Eq. (2). Therefore, the generalized DT is defined as follows:

$$\begin{aligned}\Phi_1[N-1]&=\Phi_1^{[0]}+\left[\sum_{l=1}^{N-1}T_1[l]\right]\Phi_1^{[1]}\\&+\left[\sum_{l=1}^{N-1}\sum_{k>l}^{N-1}T_1[k]T_1[l]\right]\Phi_1^{[2]}\\&+\cdots+\left[T_1[N-1]\cdots T_1[2]T_1[1]\right]\Phi_1^{[N-1]},\end{aligned} \tag{8}$$

$$q_1[N]=q_1[N-1]-3\sqrt{\frac{\alpha(t)}{\beta(t)}}(\lambda_1-\lambda_1^*)\times\frac{\varphi_1[N-1]\chi_1^*[N-1]}{|\varphi_1[N-1]|^2+|\chi_1[N-1]|^2+\left|\phi_1[N-1]^2\right|}, \tag{9a}$$

$$q_2[N]=q_2[N-1]-3\sqrt{\frac{\alpha(t)}{\beta(t)}}(\lambda_1-\lambda_1^*)\times\frac{\varphi_1[N-1]\phi_1^*[N-1]}{|\varphi_1[N-1]|^2+|\chi_1[N-1]|^2+\left|\phi_1[N-1]^2\right|}, \tag{9b}$$

where

$$T_1[k]=\lambda_1 I-H_1[k-1]\Lambda_1 H_1[k-1]^{-1},$$
$$\Phi_1[N-1]=(\varphi_1[N-1],\chi_1[N-1],\phi_1[N-1])^T,$$
$$H_1[k-1]=\begin{pmatrix}\varphi_1[k-1] & \chi_1^*[k-1] & \phi_1^*[k-1]\\ \chi_1[k-1] & -\varphi_1^*[k-1] & 0\\ \phi_1[k-1] & 0 & -\varphi_1^*[k-1]\end{pmatrix},$$

$$\Lambda_1=\begin{pmatrix}\lambda_1 & 0 & 0\\ 0 & \lambda_1^* & 0\\ 0 & 0 & \lambda_1^*\end{pmatrix}.$$

3 Dynamics of localized waves

In this section, the first- and second-order localized wave solutions of Eq. (1) are calculated, and the dynamics of localized waves are analyzed according to the evolution plots.

Assuming the plane waves $q_1[0]=a_1\sqrt{\frac{\alpha(t)}{\beta(t)}}e^{i\omega(t)}$ and $q_2[0]=a_2\sqrt{\frac{\alpha(t)}{\beta(t)}}e^{i\omega(t)}$ are seed solutions of the localized waves, where

$$\omega(t)=\int 2(a_1^2+a_2^2)\alpha(t)dt$$

and a_1 and a_2 are arbitrary real constants. The corresponding basic vector solution at λ=$\left(-\frac{2i}{3}\sqrt{a_1^2+a_2^2}\right)\left(1+\eta^2\right)$ is calculated as:

$$\Phi_1(\eta)=\begin{pmatrix}(v_1e^{\kappa_1+\kappa_2}-v_2e^{\kappa_1-\kappa_2})e^{\frac{i\omega(t)}{2}}\\ \varsigma_1(v_1e^{\kappa_1-\kappa_2}-v_2e^{\kappa_1+\kappa_2})e^{-\frac{i\omega(t)}{2}}+\varpi a_2e^{\kappa_3}\\ \varsigma_2(v_1e^{\kappa_1-\kappa_2}-v_2e^{\kappa_1+\kappa_2})e^{-\frac{i\omega(t)}{2}}-\varpi a_1e^{\kappa_3}\end{pmatrix}, \tag{10}$$

where

$$v_1=\frac{\sqrt{3\lambda-\sqrt{9\lambda^2+4(a_1^2+a_2^2)}}}{\sqrt{9\lambda^2+4(a_1^2+a_2^2)}},$$

$$v_2=\frac{\sqrt{3\lambda+\sqrt{9\lambda^2+4(a_1^2+a_2^2)}}}{\sqrt{9\lambda^2+4(a_1^2+a_2^2)}},$$

$$\kappa_1=-\frac{i\lambda}{2}\left[x+3\lambda\left(\alpha(t)+3\lambda\delta(t)\right)t\right],$$
$$\kappa_2=\frac{i}{2}\sqrt{9\lambda^2+4(a_1^2+a_2^2)}(x-\tau t+\Omega(\eta)),$$
$$\kappa_3=i\lambda\left[x+3\lambda(\alpha(t)+3\lambda\delta(t))t\right],$$
$$\tau=-3\lambda\alpha(t)+\left[2(a_1^2+a_2^2)-9\lambda^2\right]\delta(t),$$
$$\varsigma_1=\frac{ia_1}{\sqrt{a_1^2+a_2^2}},\ \varsigma_2=\frac{ia_2}{\sqrt{a_1^2+a_2^2}},\ \Omega(\eta)=\sum_{j=1}^{N}\left(m_j+in_j\right)\eta^{2j},$$

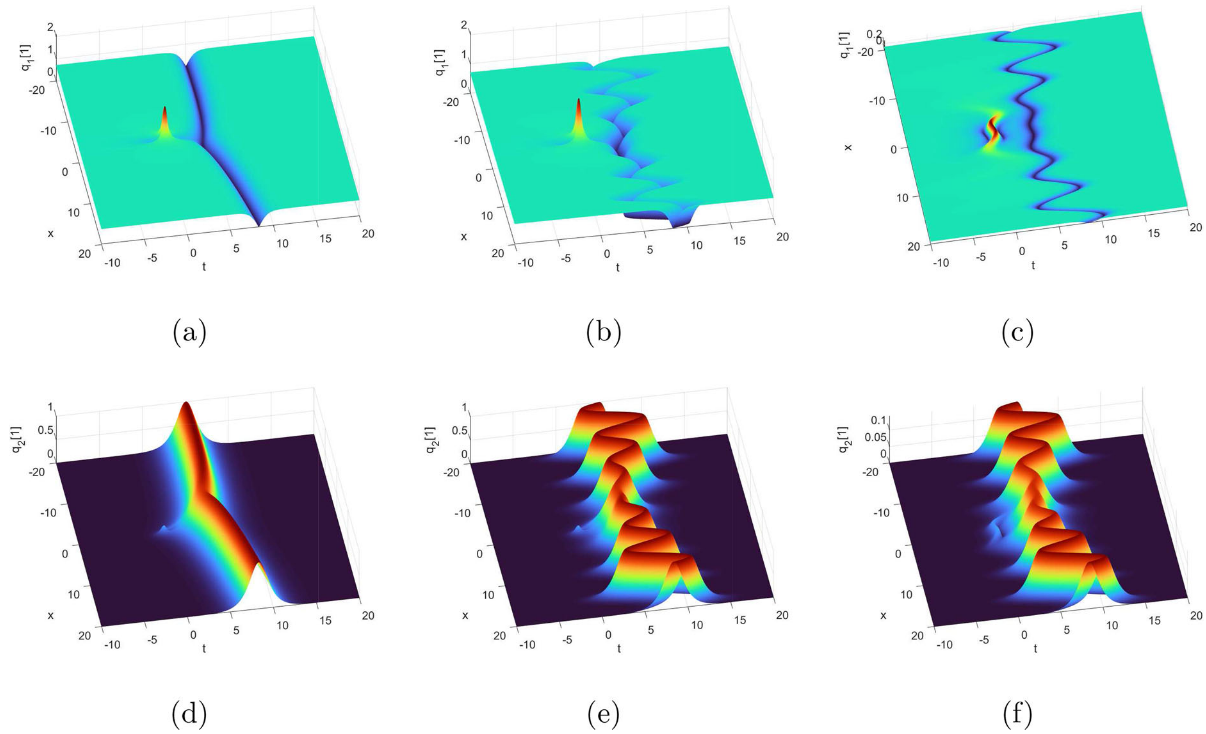

Fig. 1 The first-order localized waves with $a_1 = 1, a_2 = 0, \varpi = \frac{1}{10}$ and (**a**, **d**) $\alpha(t) = 1, \beta(t) = 2, \delta(t) = \frac{1}{50}$; (**b**, **e**) $\alpha(t) = 1, \beta(t) = 2, \delta(t) = \frac{\cos(t)}{20}$; (**c**, **f**) $\alpha(t) = \frac{t}{20}, \beta(t) = 5t, \delta(t) = \frac{\cos(t)}{20}$

in which ϖ, m_j, and n_j are arbitrary real constants.

Let $\gamma = a_1^2 + a_2^2$ and expand function $\Phi_1(\eta)$ as a Taylor series at $\eta = 0$,

$$\Phi_1(\eta) = \Phi_1^{[0]} + \Phi_1^{[1]}\eta^2 + \Phi_1^{[2]}\eta^4 + \Phi_1^{[3]}\eta^6 + \cdots, \quad (11)$$

where

$$\begin{aligned}
&\Phi_1(\eta) = \left(\varphi_1^{[k]}, \chi_1^{[k]}, \phi_1^{[k]}\right)^T \\
&= \frac{1}{(2k)!}\frac{\partial^{2k}\Phi_1}{\partial\eta^{2k}}\Big|_{\eta=0} \ (k = 0, 1, 2, \cdots), \\
&\varphi_1^{[0]} = \gamma^{-\frac{1}{4}}(-2-2i)(((i\alpha(t) \\
&\quad +3\sqrt{\gamma}\delta(t))\sqrt{\gamma}t - 2x)\sqrt{\gamma} \\
&\quad +\frac{1}{4})e^{i\gamma\int\alpha(t)dt + \frac{\sqrt{\gamma}}{3}((i\alpha(t)+2\sqrt{\gamma}\delta(t))\sqrt{\gamma}t - x)}, \\
&\chi_1^{[0]} = \gamma^{-\frac{3}{4}}(-2+2i)a_1((-\frac{x}{2} + (i\alpha(t) \\
&\quad +3\sqrt{\gamma}\delta(t))\sqrt{\gamma}t)\sqrt{\gamma} \\
&\quad -\frac{1}{4})e^{-i\gamma\int\alpha(t)dt + \frac{\sqrt{\gamma}}{3}(-x+(i\alpha(t)+2\sqrt{\gamma}\delta(t))\sqrt{\gamma}t)} \\
&\quad +2a_2\varpi\gamma e^{-\frac{2\sqrt{\gamma}}{3}(-x+2(i\alpha(t)+2\sqrt{\gamma}\delta(t))\sqrt{\gamma}t)}, \\
&\phi_1^{[0]} = \gamma^{-\frac{3}{4}}(-2+2i)a_2((-\frac{x}{2} + (i\alpha(t) \\
&\quad +3\sqrt{\gamma}\delta(t))\sqrt{\gamma}t)\sqrt{\gamma} \\
&\quad -\frac{1}{4})e^{-i\gamma\int\alpha(t)dt + \frac{\sqrt{\gamma}}{3}(-x+(i\alpha(t)+2\sqrt{\gamma}\delta(t))\sqrt{\gamma}t)} \\
&\quad -2a_1\varpi\gamma e^{-\frac{2\sqrt{\gamma}}{3}(-x+2(i\alpha(t)+2\sqrt{\gamma}\delta(t))\sqrt{\gamma}t)}.
\end{aligned}$$

As the expression $\Phi_1^{[1]} = \left(\varphi_1^{[1]}, \chi_1^{[1]}, \phi_1^{[1]}\right)^T$ is complicated, its specific form is omitted. The dynamical characteristics of the first- and second-order localized waves are discussed subsequently.

Obviously, $\Phi_1^{[0]} = (\varphi_1^{[0]}, \chi_1^{[0]}, \phi_1^{[0]})^T$ is the solution of the Lax pair when $q_1 = q_1[0]$, $q_2 = q_2[0]$, and $\lambda = -\frac{2i}{3}\sqrt{\gamma}$. According to Eqs. (8) and (9), the first-order localized wave solutions of Eq. (1) are obtained as:

$$q_1[1] = q_1[0] - 3\sqrt{\frac{\alpha(t)}{\beta(t)}}(\lambda_1 - \lambda_1^*) \times \frac{\varphi_1[0]\chi_1^*[0]}{|\varphi_1[0]|^2 + |\chi_1[0]|^2 + |\phi_1[0]|^2}, \quad (12a)$$

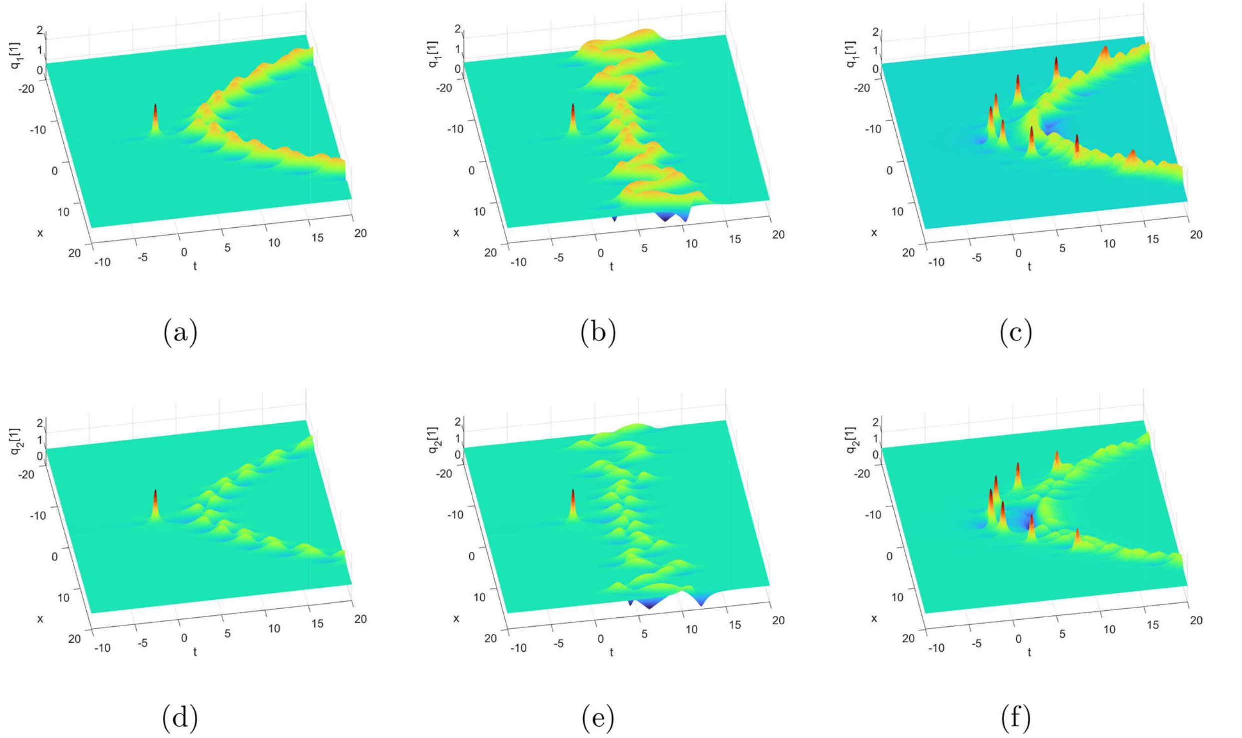

Fig. 2 The first-order localized waves with $a_1 = \frac{4}{5}, a_2 = 1, \varpi = \frac{1}{100}$ and (**a**, **d**) $\alpha(t) = \frac{3}{2}, \beta(t) = \frac{3}{2}, \delta(t) = \frac{t}{100}$; (**b**, **e**) $\alpha(t) = \frac{3}{2}, \beta(t) = \frac{3}{2}, \delta(t) = \frac{\sin(t)}{30}$; (**c**, **f**) $\alpha(t) = \frac{\sin(t)}{3}, \beta(t) = \frac{\sin(t)}{3}, \delta(t) = \frac{t}{100}$

$$q_2[1] = q_2[0] - 3\sqrt{\frac{\alpha(t)}{\beta(t)}}(\lambda_1 - \lambda_1^*) \times \frac{\varphi_1[0]\phi_1^*[0]}{|\varphi_1[0]|^2 + |\chi_1[0]|^2 + |\phi_1[0]|^2}, \tag{12b}$$

The evolution plots of the first-order localized waves are obtained by altering the values of the free parameters. The dynamics of the first-order localized waves are then discussed.

Figure 1 depicts the interactions between first-order rogue waves and dark-bright solitons. When $\alpha(t)$, $\beta(t)$, and $\delta(t)$ are constants, the first-order rogue wave in the component $q_1[1]$ interacts with one dark soliton and the velocity of the dark soliton remains constant during propagation, as shown in Fig. 1a. When $\alpha(t)$ and $\beta(t)$ are constants and $\delta(t) = \frac{\cos(t)}{20}$, the first-order rogue wave will interact with the periodic dark soliton, as shown in Fig. 1b. When $\alpha(t)$ and $\beta(t)$ are variable coefficients and $\delta(t) = \frac{\cos(t)}{20}$, unlike the previous plots, the rogue wave changes into an S-shape, as shown in Fig. 1c. Figure 1d–f shows that the rogue wave in the component $q_2[1]$ is not easily observed in a background of zero amplitude.

Figure 2 shows the collision between a first-order rogue wave and one breather. Figure 2a and d displays the first-order rogue wave coexisting with a parabolic breather when $\alpha(t)$ and $\beta(t)$ are constants, and $\delta(t)$ is a linear function. Figure 2b and e shows the evolution plots of the first-order rogue wave interacting with the periodic breather when $\alpha(t)$ and $\beta(t)$ are the same as the former and $\delta(t)$ is a trigonometric function. Figure 2c and f illustrates the presence of periodic rogue waves, which are observed when $\alpha(t)$ and $\beta(t)$ are trigonometric functions and $\delta(t) = \frac{t}{100}$. Moreover, Fig. 2 illustrates that the amplitude of $q_1[1]$ is greater than the amplitude of $q_2[1]$, which are both influenced by a_1 and a_2.

Based on the following limit formula

$$\Phi_1[1] = \lim_{\eta\to 0} \frac{T[1]\big|_{\lambda=\lambda_1(1+\eta^2)}\Phi_1}{\eta^2} = \lim_{\eta\to 0} \frac{(\lambda_1\eta^2 + T_1[1]\big|_{\lambda=\lambda_1})\Phi_1}{\eta^2} = \lambda_1\Phi_1^{[0]} + T_1[1]\Phi_1^{[1]}, \tag{13}$$

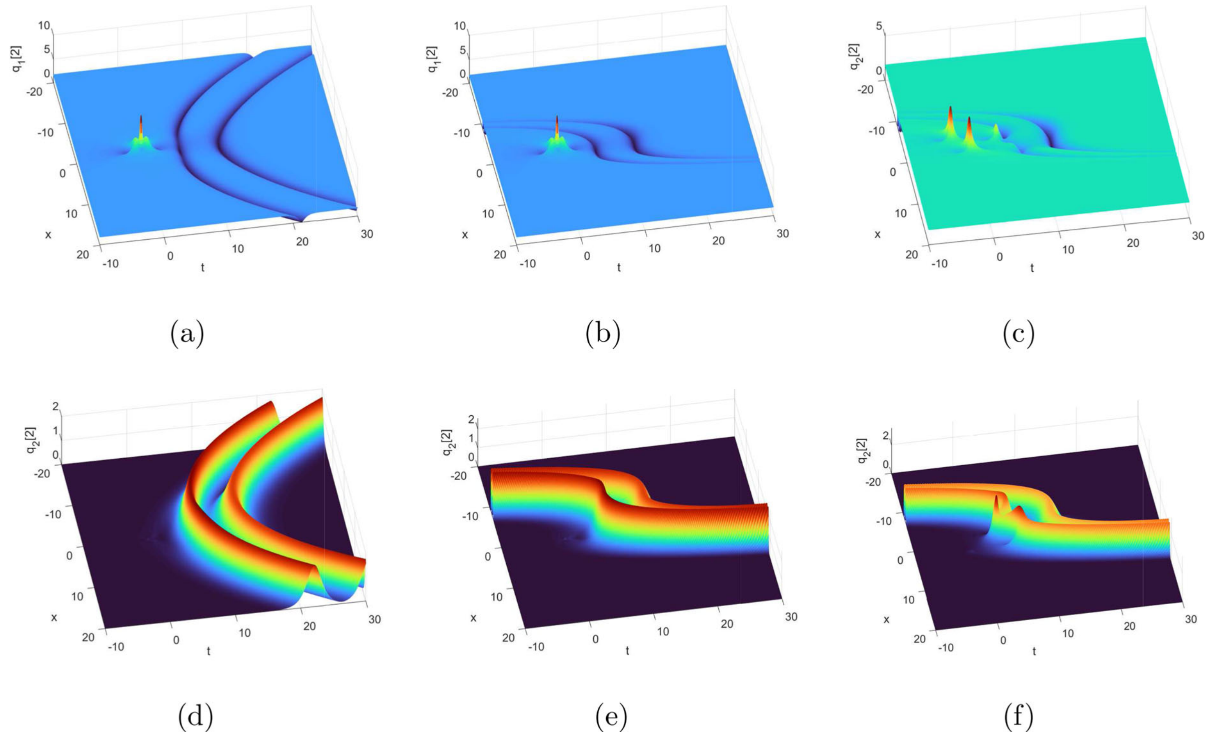

Fig. 3 The second-order localized waves with $a_1 = 1, a_2 = 0, \alpha(t) = 1, \beta(t) = \frac{1}{3}, \varpi = \frac{1}{100}$ and (**a**, **d**) $\delta(t) = \frac{t}{100}, m_1 = 0, n_1 = 0$; (**b**, **e**) $\delta(t) = \frac{t^2}{100}, m_1 = 0, n_1 = 0$; (**c**, **f**) $\delta(t) = \frac{t^2}{100}, m_1 = 30, n_1 = 30$

and Eqs. (8) and (9), the second-order localized wave solutions can be obtained as:

$$q_1[2] = q_1[1] - 3\sqrt{\frac{\alpha(t)}{\beta(t)}}(\lambda_1 - \lambda_1^*) \times \frac{\varphi_1[1]\chi_1^*[1]}{|\varphi_1[1]|^2 + |\chi_1[1]|^2 + |\phi_1[1]|^2}, \tag{14a}$$

$$q_2[2] = q_2[1] - 3\sqrt{\frac{\alpha(t)}{\beta(t)}}(\lambda_1 - \lambda_1^*) \times \frac{\varphi_1[1]\phi_1^*[1]}{|\varphi_1[1]|^2 + |\chi_1[1]|^2 + |\phi_1[1]|^2}, \tag{14b}$$

where

$$\Phi_1[1] = (\varphi_1[1], \chi_1[1], \phi_1[1])^T,$$
$$T_1[1] = \lambda_1 I - H_1[0]\Lambda_1 H_1[0]^{-1},$$
$$H_1[0] = \begin{pmatrix} \varphi_1[0] & \chi_1^*[0] & \phi_1^*[0] \\ \chi_1[0] & -\varphi_1^*[0] & 0 \\ \phi_1[0] & 0 & -\varphi_1^*[0] \end{pmatrix},$$
$$\Lambda_1 = \begin{pmatrix} \lambda_1 & 0 & 0 \\ 0 & \lambda_1^* & 0 \\ 0 & 0 & \lambda_1^* \end{pmatrix}.$$

Similarly, the dynamical characteristics of the second-order localized wave solutions are analyzed by altering the values of the free parameters in the following cases.

Figure 3a and d exhibits the second-order rogue wave interacting with two parabolic dark-bright solitons and displays the parabolic dark-bright solitons' accelerating and decelerating motions when $\alpha(t)$ and $\beta(t)$ are constants, $\delta(t) = \frac{t}{100}$, $m_1 = 0$, and $n_1 = 0$. When $\delta(t) = \frac{t^2}{100}$, $m_1 = 0$, and $n_1 = 0$, the dark solitons change from parabolic to cubic, as shown in Fig. 3b. Unlike the former, in Fig. 3c, the second-order rogue wave is separated into three first-order rogue waves when $m_1 = 30$ and $n_1 = 30$. This result indicates that the amplitude of the separated second-order rogue wave becomes smaller and its energy is lower than that of the second-order one without separation. Furthermore, the rogue wave in the component $q_2[2]$ is difficult to observe in a background of zero amplitude, as shown in Fig. 3d–f.

Figure 4 shows the dynamics of the second-order rogue wave and breathers when $\alpha(t)$ and $\beta(t)$ are constants and $\delta(t)$ is a trigonometric function. Figure 4a

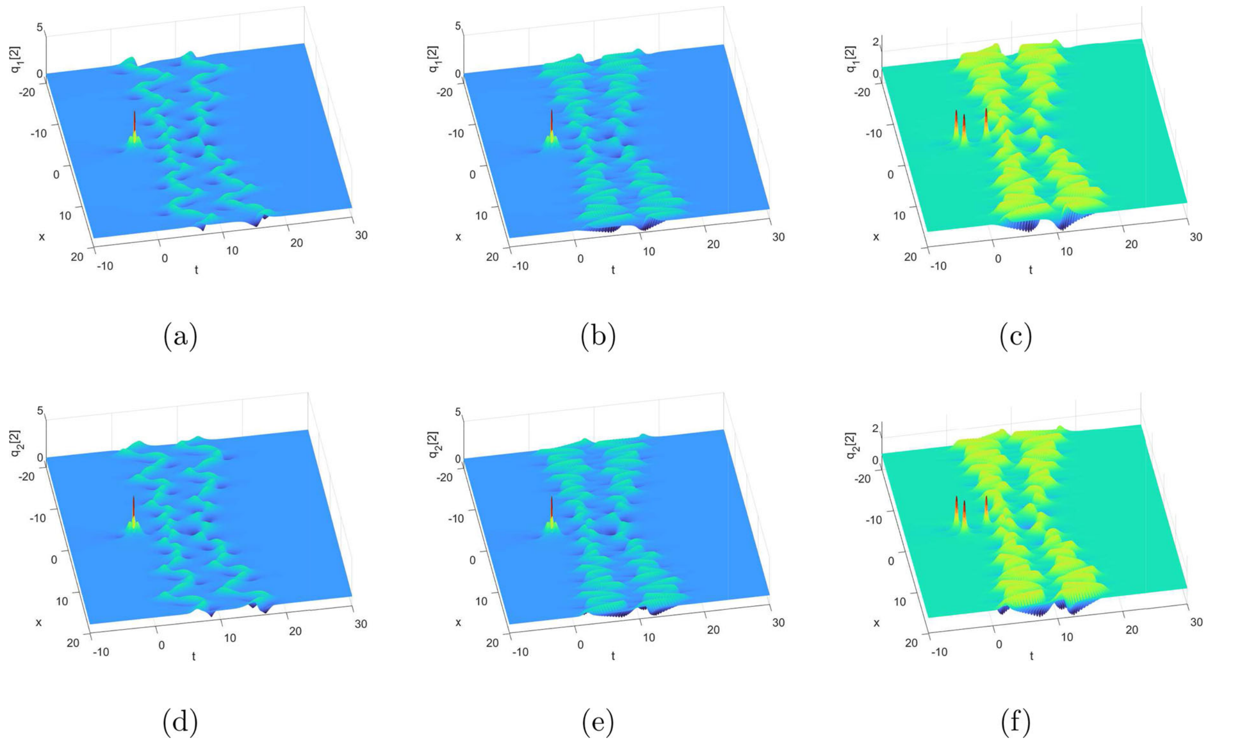

Fig. 4 The second-order localized waves with $a_1 = 1$, $a_2 = 1$, $\alpha(t) = 1$, $\beta(t) = 1$, $\varpi = \frac{1}{1000}$ and (**a**, **d**) $\delta(t) = \frac{\cos(t)}{50}$, $m_1 = 0$, $n_1 = 0$; (**b**, **e**) $\delta(t) = \frac{\cos(3t)}{50}$, $m_1 = 0$, $n_1 = 0$; (**c**, **f**) $\delta(t) = \frac{\cos(3t)}{50}$, $m_1 = 20$, $n_1 = 20$

and d displays the second-order rogue wave interacting with two periodic breathers when $\delta(t) = \frac{\cos(t)}{50}$, $m_1 = 0$, and $n_1 = 0$. Based on the above parameters, the period of the two breathers decreases, and their propagation velocity becomes faster when $\delta(t) = \frac{\cos(3t)}{50}$, as illustrated in Fig. 4b and e. Compared with Fig. 4a and d, b and e indicate that $\delta(t)$ has no effect on the amplitude of the breathers and changes the propagation velocity of the breathers. In addition, Fig. 4c and f shows that separation phenomenon occurs in the second-order rogue waves when changing the values of parameters m_1 and n_1.

Figure 5a demonstrates that the second-order rogue wave coexists with the two periodic parabolic dark solitons when $\alpha(t)$ and $\beta(t)$ are constants and $\delta(t) = \frac{t+\cos(5t)}{30}$. Furthermore, it is found that $\delta(t)$ determines the type of dark soliton. The second-order rogue wave and the two dark solitons are periodic when $\alpha(t)$, $\beta(t)$, and $\delta(t)$ are trigonometric functions, and the height of the rogue waves' peak decreases along the positive and negative directions of the x axis (as shown in Fig. 5b). It is hard to observe the second-order rogue when the second-order rogue wave is together with bright solitons, as illustrated in Fig. 5c and d.

When $\alpha(t)$ and $\beta(t)$ are variable coefficients, $\delta(t)$ is a constant, $m_1 = 0$, and $n_1 = 0$, the second-order rogue wave and K-shape dark-bright solitons are generated together, as shown in Fig. 6a and c. Figure 6b illustrates that the second-order rogue wave is separated into three first-order rogue waves when the values of m_1 and n_1 are changed. It is also found that the rogue wave is difficult to identify when $a_2 = 0$ in the component $q_2[2]$.

4 Conclusions

This work studied a variable-coefficient coupled Hirota equation by constructing generalized DT on the basis of classical DT and Taylor expansion. The equation was then used to obtain first- and second-order localized wave solutions, whereby localized wave evolution plots were obtained via numerical simulation. It was found that the parameters had an important effect

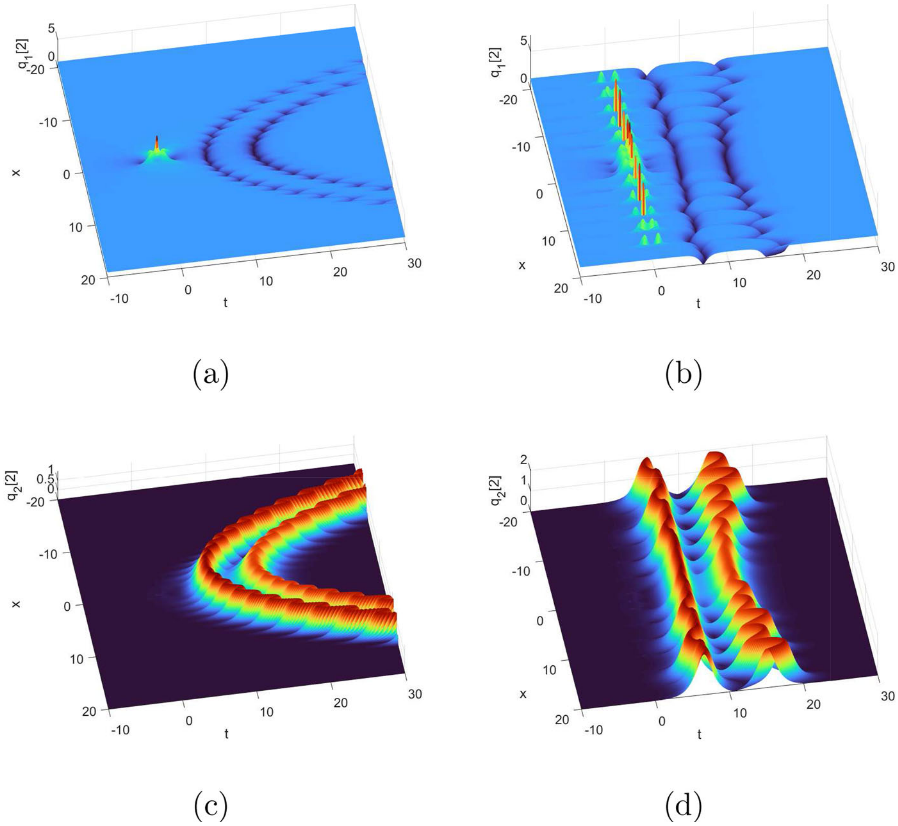

Fig. 5 The second-order localized waves with $a_1 = 1, a_2 = 0, \varpi = \frac{1}{200}, m_1 = 0, n_1 = 0$ and (**a**, **c**) $\alpha(t) = 1, \beta(t) = 1, \delta(t) = \frac{t+\cos(5t)}{30}$; (**b**, **d**) $\alpha(t) = \cos(t), \beta(t) = \frac{\cos(t)}{2}, \delta(t) = \frac{\cos(t)}{80}$

on the dynamics of the localized waves. The parameters a_1 and a_2 had a significant influence on the type of localized waves. If $a_1 \neq 0$ and $a_2 = 0$, the rogue waves coexisted with dark-bright solitons; if a_1 and a_2 were not equal to 0, the rogue waves interacted with breathers. The parameters m_j and n_j $(j = 1, 2, \cdots, N-1)$ determined the separation of the rogue waves. When the parameters m_1 and n_1 were not equal to 0, the second-order rogue waves separated into three first-order rogue waves. Moreover, it was observed that the functions$\alpha(t)$, $\beta(t)$, and $\delta(t)$ influenced the propagation shape of localized waves. When $\alpha(t)$, $\beta(t)$, and $\delta(t)$ were constants, common localized waves occurred. When $\alpha(t)$ and $\beta(t)$ were constants and $\delta(t)$ was a linear, quadratic, or trigonometric function, the rogue waves interacted with the parabolic, cubic, or periodic dark-bright solitons and breathers. When $\alpha(t)$, $\beta(t)$, and $\delta(t)$ were trigonometric functions, the localized waves had periodicity all along the propagation direction. These results contribute to the understanding of localized wave propagation in inhomogeneous optical fibers.

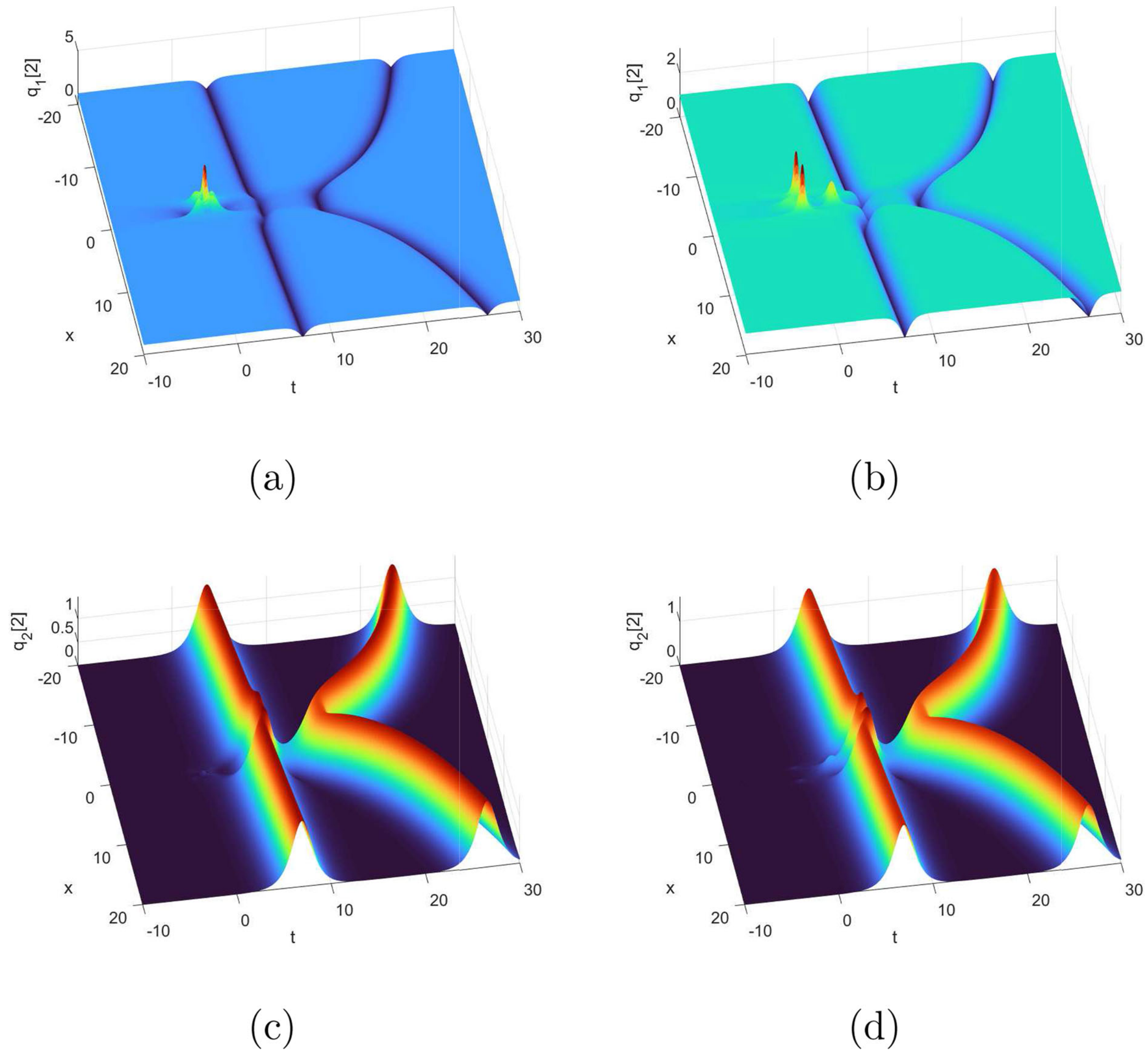

Fig. 6 The second-order localized waves with $a_1 = 1, a_2 = 0, \alpha(t) = t, \beta(t) = t, \delta(t) = \frac{1}{50}, \varpi = \frac{1}{100}$ and (**a**, **c**) $m_1 = 0, n_1 = 0$; (**b**, **d**) $m_1 = 10, n_1 = 10$

Acknowledgements The authors sincerely thanks for the support of the National Natural Science Foundation of China (NNSFC) through grant No. 11602232, Research Project Supported by Shanxi Scholarship Council of China through grant No. 2022-150 and Natural Science Foundation of Shanxi Province through grant No. 202203021211086 and No. 202203021211088.

Data Availability Data sharing does not apply to this article as no data sets were generated or analyzed during the current study.

Declarations

Conflict of interest The authors declare that they have no conflicts of interest to report regarding the present study.

References

1. Boscolo, S., Finot, C.: Artificial neural networks for nonlinear pulse shaping in optical fibers. Opt. Laser Technol. **131**, 106439 (2020)
2. Iida, D., Honda, N., Oshida, H.: Advances in distributed vibration sensing for optical communication fiber state visualization. Opt. Fiber Technol. **57**, 102263 (2020)
3. Ma, G.L., Zhao, J., Zhou, Q., et al.: Soliton interaction control through dispersion and nonlinear effects for the fifth-order nonlinear Schrödinger equation. Nonlinear Dyn. **106**(3), 2479–2484 (2021)
4. Wang, S., Fang, N., Wang, L.: Signal recovery based on optoelectronic reservoir computing for high speed optical

fiber communication system. Opt. Commun. **495**, 127082 (2021)
5. Kaur, S., Singh, P., Tripathi, V., et al.: Recent trends in wireless and optical fiber communication. In: Global Transitions Proceedings (2022)
6. Ali, F., Jhangeer, A., Muddassar, M., et al.: Solitonic, quasi-periodic, super nonlinear and chaotic behaviors of a dispersive extended nonlinear Schrödinger equation in an optical fiber. Results Phys. **31**, 104921 (2021)
7. Wazwaz, A.M., Albalawi, W., El-Tantawy, S.A.: Optical envelope soliton solutions for coupled nonlinear Schrödinger equations applicable to high birefringence fibers. Optik **255**, 168673 (2022)
8. Yan, X.W., Chen, Y.: Soliton interaction of a generalized nonlinear Schrödinger equation in an optical fiber. Appl. Math. Lett. **125**, 107737 (2022)
9. Parasuraman, E.: Soliton solutions of Kundu-Eckhaus equation in birefringent optical fiber with inter-modal dispersion. Optik **223**, 165388 (2020)
10. Triki, H., Sun, Y., Biswas, A., et al.: On the existence of chirped algebraic solitary waves in optical fibers governed by Kundu-Eckhaus equation. Results Phys. **34**, 105272 (2022)
11. Rehman, S.U., Ahmad, J.: Modulation instability analysis and optical solitons in birefringent fibers to RKL equation without four wave mixing. Alex. Eng. J. **60**(1), 1339–1354 (2021)
12. Yan, Y., Liu, W., Zhou, Q., et al.: Dromion-like structures and periodic wave solutions for variable-coefficients complex cubic-quintic Ginzburg-Landau equation influenced by higher-order effects and nonlinear gain. Nonlinear Dyn. **99**(2), 1313–1319 (2020)
13. Muniyappan, A., Monisha, P., Nivetha, V.: Generation of wing-shaped dark soliton for perturbed Gerdjikov-Ivanov equation in optical fiber. Optik **230**, 166328 (2021)
14. Osman, M.S., Almusawa, H., Tariq, K.U., et al.: On global behavior for complex soliton solutions of the perturbed nonlinear Schrödinger equation in nonlinear optical fibers. J. Ocean Eng. Sci. (2021)
15. Zayed, E.M.E., Alngar, M.E.M., Shohib, R.M.A., et al.: Highly dispersive optical solitons in birefringent fibers for perturbed complex Ginzburg-Landau equation having polynomial law of nonlinearity. Optik **261**, 169206 (2022)
16. Li, B.Q., Ma, Y.L.: Periodic and N-kink-like optical solitons for a generalized Schrödinger equation with variable coefficients in an inhomogeneous fiber system. Optik **179**, 854–860 (2019)
17. El-Shiekh, R.M.: Classes of new exact solutions for nonlinear Schrödinger equations with variable coefficients arising in optical fiber. Results Phys. **13**, 102214 (2019)
18. Lan, Z.Z.: Soliton and breather solutions for a fifth-order variable-coefficient nonlinear Schrödinger equation in an optical fiber. Appl. Math. Lett. **102**, 106132 (2020)
19. Maddouri, K., Azzouzi, F., Triki, H., et al.: Dark-managed solitons in inhomogeneous cubic-quintic-septimal nonlinear media. Nonlinear Dyn. **103**(3), 2793–2803 (2021)
20. Khalifa, S.B., Chebaane, S., Nayagam, V.S., et al.: Periodic and nonperiodic amplifications of attosecond solitons in an inhomogeneous lossy optical fiber. Optik **252**, 168498 (2022)
21. Liu, J.G., Xiong, W.P.: Multi-wave, breather wave and lump solutions of the Boiti-Leon-Manna-Pempinelli equation with variable coefficients. Results Phys. **19**, 103532 (2020)
22. Sakkaravarthi, K., Kanna, T., Mareeswaran, R.B.: Higher-order optical rogue waves in spatially inhomogeneous multimode fiber. Physica D **435**, 133285 (2022)
23. Ma, Y.L.: Nth-order rogue wave solutions for a variable coefficient Schrödinger equation in inhomogeneous optical fibers. Optik **251**, 168103 (2022)
24. Song, J.Y., Hao, H.Q., Zhang, X.M.: Discrete soliton solutions for a generalized discrete nonlinear Schrödinger equation with variable coefficients via discrete N-fold Darboux transformation. Appl. Math. Lett. **78**, 126–132 (2018)
25. Wang, X., Wang, L.: Darboux transformation and nonautonomous solitons for a modified Kadomtsev-Petviashvili equation with variable coefficients. Comput. Math. Appl. **75**(12), 4201–4213 (2018)
26. Xin, X., Xia, Y., Liu, H., et al.: Darboux transformation of the variable coefficient nonlocal equation. J. Math. Anal. Appl. **490**(1), 124227 (2020)
27. Luo, L.: Bäcklund transformation of variable-coefficient Boiti-Leon-Manna-Pempinelli equation. Appl. Math. Lett. **94**, 94–98 (2019)
28. Li, L.Q., Gao, Y.T., Yu, X., et al.: Bilinear forms, bilinear Bäcklund transformation, soliton and breather interactions of a damped variable-coefficient fifth-order modified Korteweg-de Vries equation for the surface waves in a strait or large channel. Chin. J. Phys. **77**, 915–926 (2022)
29. Zeynel, M., Yaşar, E.: A new (3+ 1) dimensional Hirota bilinear equation: Periodic, rogue, bright and dark wave solutions by bilinear neural network method. J. Ocean Eng. Sci. (2022)
30. Raza, N., Rafiq, M.H., Kaplan, M., et al.: The unified method for abundant soliton solutions of local time fractional nonlinear evolution equations. Results Phys. **22**, 103979 (2021)
31. Yang, D.Y., Tian, B., Tian, H.Y., et al.: Darboux transformation, localized waves and conservation laws for an M-coupled variable-coefficient nonlinear Schrödinger system in an inhomogeneous optical fiber. Chaos Solitons Fractals **156**, 111719 (2022)
32. Triki, H., Zhou, Q., Biswas, A., et al.: Localized pulses in optical fibers governed by perturbed Fokas-Lenells equation. Phys. Lett. A **421**, 127782 (2022)
33. Wang, M., Tian, B.: Lax Pair, Generalized Darboux Transformation, and Solitonic Solutions for a Variable-Coefficient Coupled Hirota System in an Inhomogeneous Optical Fiber. Rom. J. Phys. **66**, 119 (2021)
34. Wang, X., Liu, C., Wang, L.: Darboux transformation and rogue wave solutions for the variable-coefficients coupled Hirota equations. J. Math. Anal. Appl. **449**(2), 1534–1552 (2017)
35. Guan, W.Y., Li, B.Q.: Controllable managements on the optical vector breathers in a coupled fiber system with multiple time-dependent coefficients. Optik **206**, 164309 (2020)
36. Shi, Z., Gao, B.: On complex wave solutions depicted by the variable coefficients coupled Hirota equation. Optik **242**, 167123 (2021)
37. Yang, D.Y., Tian, B., Qu, Q.X., et al.: Lax pair, conservation laws, Darboux transformation and localized waves of a variable-coefficient coupled Hirota system in an inhomo-

geneous optical fiber. Chaos Solitons Fractals **150**, 110487 (2021)
38. Yang, D.Y., Tian, B., Tian, H.Y., et al.: Interaction between the breather and breather-like soliton, and breather-to-soliton conversions of a variable-coefficient coupled Hirota system in an inhomogeneous optical fiber. Optik **247**, 166815 (2021)
39. Li, B.Q., Ma, Y.L.: Interaction properties between rogue wave and breathers to the manakov system arising from stationary self-focusing electromagnetic systems. Chaos Solitons Fractals **156**, 111832 (2022)
40. Li, B.Q., Ma, Y.L.: A 'firewall' effect during the rogue wave and breather interactions to the Manakov system. Nonlinear Dyn. https://doi.org/10.1007/s11071-022-07878-6 (2022)
41. Sun, J.Z., Li, B.Q., Ma, Y.L.: Phase complementarity and magnification effect of optical pump rogue wave and Stokes rogue wave in a transient stimulated Raman scattering system. Optik **269**, 169869 (2022)
42. Rajan, M., Hakkim, J., Mahalingam, A., et al.: Dispersion management and cascade compression of femtosecond nonautonomous soliton in birefringent fiber. Eur. Phys. J. D **67**(7), 1–8 (2013)